

Chapter 1

Introduction to Nonthermal Atmospheric Pressure Plasma: Physical and Chemical Basis



Alexander A. Fridman, Michael Keidar, and Eun Ha Choi

Abstract Plasma bioscience and medicine today is an interdisciplinary division of modern science and technology. It includes fundamental physics essential to develop new plasma sources and its diagnostics applicable for biological applications, clinical treatments, medicine to apply the technology not only on cells but also on the whole organism and medical testing, and finally bioscience and environmental issues. Nonthermal atmospheric pressure plasma can be efficacious in several biological applications such as blood coagulation treatment, sterilization, tissue bioengineering, modification of biomaterials, wound healing, agriculture, food processing, eradication of environmental issues, and various other applications. It is important to note that this chapter explained the safety and stability of plasma devices used for various applications, which is the main concern in this developing field. In the first part, the history of plasma bioscience and medicine area including clinical trials in cancer and other diseases is included. Specifically, in this chapter detailed diagnostic procedures for various plasma sources and plasma-based substances are incorporated. The last section of this chapter described optical emission spectroscopy (OES) for the reactive species detection, measurement of the plasma electron density and temperatures by interferometry and collisional radiative models, and rotational and vibrational temperatures of molecules in plasma gases by using an Boltzman plot from optical spectroscopy, the plasma radical densities by absorption spectroscopy method, and the plasma parameters for industry biomedical plasma products.

A. A. Fridman
Nyheim Plasma Institute, Drexel University, Philadelphia, USA

M. Keidar
Mechanical and Aerospace Engineering Department, George Washington University, Washington, DC, USA

E. H. Choi (✉)
Plasma Bioscience Research Center (PBRC), Department of Electrical and Biological Physics, Kwangwoon University, Wolgye Dong, Nowon Gu, 01897 Seoul, South Korea
e-mail: ehchoi@kw.ac.kr

1.1 Introduction to Plasma Bioscience and Medicine

1.1.1 Plasma Medicine is a New Division of Medical Science and Technology

Innovative concepts in medical technology give new possibilities: plasma bioscience and medicine are certainly one of those hopes. Latest advancements in physics and engineering have stemmed in several crucial clinical developments. Among several clinical strategies that have been extensively reported in the earlier literature are administration of high energy radiations, ultrasound, lasers, electromagnetic waves. Plasma based strategies are comparatively newbie in the medical areas. Latest exponential advances in electrical physics and engineering endorsed subsequent considerable developments in the cold atmospheric pressure plasma area. Space-uniform and controlled nonthermal atmospheric plasma devices turn out to be a reality. All that created a prospect to safe and control application of plasma to organisms. All that stimulated innovation of a new thrilling field of medicine—plasma medicine. Investigations performed at various main academics and hospitals across the world since from a decade shows that nonthermal plasma can deliver innovative solutions of tricky health issues. Plasma is efficient in decontamination of various surfaces as well as living tissues, sterilizes large amount of air and water, neutralizes hazardous microbes together with those in food materials, and capable to halt severe hemorrhage without affecting normal tissue. Plasma can be precisely utilized to induce wound healing and to cure various diseases such as cancer, disorders related to various other human body parts and organs. Nonthermal plasma is also shown to be efficient in blood treatment to regulate properties of blood. It is also proved to be effective in surface exposure for modification of various biological materials and subjects, in diagnostics and even in pharma field by modifying characteristics of existing drug molecules and producing a new one. These plasma discharges, significantly established lately due to the promising developments in electronic engineering areas, is obviously a potential tool to be delivered to health professionals for solving clinical problems earlier unresolved. This is a foundation of great attention at the moment to the plasma medicine, which is the subject of this article.

1.1.2 Controllability and Safety of Plasma

While discussing about the new plasma devices which are likely to be utilized to humans, also for exposure of biological subjects in biomedical investigations, plasma physicist must emphasize “controllability” and “safety” of these plasma sources. For instance, the floating electrode dielectric barrier discharge plasma (FE-DBD) device extensively utilized for clinical utilization, in Nyheim Plasma Institute, applies about 30–40 kV precisely to body (for example a photo of one of the founders of plasma

bioscience and medicine with FE-DBD discharge, Fig. 1.1, [1]). Figure 1.2 illustrates interaction of the DBD-based plasma jet with human body.

Definitely, “safety” and “controllability” of the plasma parameters are main concern in this case. The uniform plasmas together with plasma based medical sources established lately can be efficiently monitored and controlled, which is critical for maintaining doses of clinical treatment, and also for mechanism. With physical, chemical, and biological mechanisms understanding, plasma technology has plenty of opportunities for effective therapies in clinics.

Plasma is indeed far from thermodynamic equilibrium. This non-equilibrium ionized gas can be extremely “innovative” in contact with biological factors. As it was originally shown in 1950s by Stanley Miller (Fig. 1.3) and other group members, this discharge is capable to produce amino acids from methane and inorganic compounds.

Fig. 1.1 Non-thermal 40 kV FE-DBD plasma was maintained right between an electrode and a person



Fig. 1.2 DBD-based atmospheric pressure plasma jet interacting with skin





Fig. 1.3 Stanley Miller from University of Chicago in 1950s produced amino acids using inorganic compounds and methane with plasma

It is quite feasible that nonthermal plasma as multi-parametric and strongly non-equilibrium can be important for origin of life. Latest investigations demonstrate regulated modifications of DNA after the plasma exposure extremely susceptible to physical and chemical parameters of plasma. It describes the exceptional significance of the “controllability” of physical factors and intense knowledge of processes for fruitful development of the plasma medicine area. Accomplishment of plasma technologies needs thorough knowledge of chemical, physician and biological mechanisms of the discharge interaction with biological subjects. Short of basic knowledge of physics, chemistry and biology, the plasma medicine is under the risks of turn into a modernized medieval magic (see Fig. 1.4).

1.1.3 Plasma Application to Biology and Medicine from the Very First Steps Till Today

Earlier, it was observed that discharges in ambience outcome in “strange smells” affecting organism, and humans. These concepts and explanations, which are far older than *plasma bioscience* and *plasma physics* concept itself, can be credited to



Fig. 1.4 Son of Frankenstein, 1939, operating kind of gliding arc discharge plasma

investigation of famous chemist Martinus van Marum in year 1785 with discharges on water. A famous German chemist Christian Friedrich Schönbein detected production of the similar “strange pungent smell” and identified it as ball lightning. He separated in 1839 the gaseous species accountable for this “unusual smell” and known as “ozone”. This ionized gas applications in bioscience have been considerably intensify in 1850s when Werner von Siemens initially used dielectric barrier discharge to produce ozone for disinfection of water. Big scale of plasma-based sterilization or disinfection has been realized few decades later, when the first plasma plant for water supply was constructed in France Nice city. Remarkably, ozone was believed as an electric discharge-based constituent: A California city even had as its formal saying “Beaumont: Zone of Ozone” at that time.

First plasma discharge utilization to cure diseases can be credited to investigation of French researcher Jacques-Arsène d’Arsonval in 1900s, as shown in Fig. 1.5. The appropriate sources had been made possible by Nikola Tesla, who performed with exceptionally high-frequency currents at high voltage, producing “remarkable light phenomena which demonstrated safe to human being for direct exposure or treatments”.

In early of 1900s in Germany, the plasma sources were more established for the caloric treatment of humans (diathermy). A german researcher Rumpf created a source which differed as of the French ones by applying a capacitively coupled electrode comprising of a Leydener bottle which was exposed to skin of human. This plasma source can be deemed the first dielectric barrier discharge source in plasma medicine. In the beginning of 1920s, thermal electrosurgical sources and then argon gas based plasma coagulator became an significant move in clinical uses of plasma.

Fig. 1.5 First “pre-historic” steps of plasma medicine



Crucial preliminary progress in this path is linked to investigations of well known American researcher William Bowie in 1920s.

In beginning of 1960s, patent reports and publications in journals began to emerge around the world with a emphasis on nonthermal plasma decontamination, sterilization, regulation of bioactivity of microbes, as well as properties of polymer biomaterials. Several relevant literatures started increasing in beginning of 1990s, also several results presented in international conference at that time. On the basis of these preliminary achievements, as well as revolutionary progress of new plasma sources capable to be treat human body in clinics, the novel area of PLASMA MEDICINE was born in early 2000s.

Plasma medicine today is an interdisciplinary division of science and engineering. It includes physics essential to establish new plasma sources applicable for clinical treatments, medicine to apply on human patients and testing, and finally bioscience to acknowledge complicated biological processes and pathways involved in the treatment. Brief review cannot describe major achievements of the plasma medical technology and related fields of plasma agriculture and food processing. The detailed information on plasma medicine fundamentals and applications can be found in the major reviews and books of Fridman et al. [2], Laroussi et al. [3], Fridman and Friedman [1], Metelmann et al. [4], Toyokuni et al. [5], Keidar et al. [6], Kuo [7], Lu et al. [8], Keidar [9].

1.1.4 Plasma as a Helpful Tool for Medicine, Electric Discharges in Plasma Medicine

Nonthermal plasmas are capable to generate high level of reactive species (e. g. electrons, ions, atoms and radicals, excited atoms and molecules, and photons with wide range). Large amount of reactive species are important for plasma uses as plasma-based ignition and combustion, and plasma based ozone formation for water disinfection. In clinical settings, production of the high-level active species can be important, such as, for decontamination, and tissue bioengineering.

Cold plasmas, offering high concentration of the reactive species at room temperature. This characteristic regulates elitism of plasma usage in electronics productions: several components of advance computers, mobile phones, tv panels (including plasma panel), and various other electronic devices are produced applying nonthermal plasma technology. This crucial property also establishes extensive usage of nonthermal plasma in treatment of biomaterials such as polymers: textiles, photographic sheets, packaging materials and many other applications. In clinical settings, plasma generated high concentration of active species can be interesting, for instance, for blood coagulation and modifications of blood components, disinfection of skin and tissues, and ultimately wound healing and various disorders not efficiently cured earlier. these definite plasma characteristics mentioned above permit important alteration of traditional chemical and bio-chemical processes, permit crucial intensification of their effectiveness, and efficacious to stimulate biochemical reactions that cannot be achieved by traditional technologies.

Hot and cold plasmas both are very important for bio-medical applications. High temperatures and energy densities characteristic for hot plasmas reveal their uses for cauterization and tissue removal in the course of surgical procedure. These sources extensively utilized currently in clinical procedure, including tissue disinfection. Hot plasma in air also is very important to generate nitric oxide (NO), which establishes its use in the treatment of wounds and various other diseases. As mentioned above, cold plasma facilitates production of exceptionally high concentration of the reactive species, while keeping bulk temperatures as low as ambient temperature. It regulates particular niche of the cold plasma, which is generally blood coagulation and sterilization of skin and tissues, disinfection of clinical tools and materials and devices, treating of polymers, tissue engineering, and conclusively various illnesses not successfully cured earlier.

Mainly plasma based biomedical applications need operation at ambient pressure, thus necessitate usage of atmospheric pressure plasma devices. The corona discharge is well-known type of plasma. Corona discharge electron temperature is more than 1 eV, however gas temperature stays around room temperature. These plasmas are, specifically utilized in treatment of polymers such as fabrics to support appropriate adhesion before applying dyes.

Atmospheric pressure cold plasmas can be efficacious in blood coagulation and treatment, sterilization, tissue bioengineering, modification of biomaterials, wound healing, and various other diseases treatment. It is crucial to understand the safety

of the device, not corona but more complex plasma sources such as DBD plasma or Jet plasma used for various biomedical applications (see Figs. 1.1 and 1.2).

1.1.5 Plasma Chemistry: A Basic Foundation

Nonthermal plasma is a multicomponent system that is extremely active due to a large amount of charged particles, excited atoms and molecules, reactive oxygen and nitrogen species, and UV photons. Every plasma constituent performs its function in plasma-based chemical kinetics. Such as electrons are typically first to get the energy from the electric field and then disseminate it to other constituents. Varying parameters of the electron gas density, temperature, and electron energy distribution function usually allow a way to regulate plasma-based chemical reactions.

Ions are heavy particles, which are capable of give a major influence on plasma-based chemical kinetics due to their capability to put down reaction activation barriers. This feature is responsible for so-called plasma catalysis, which is especially critical in plasma-based combustion, hydrogen production, fuel conversion, exhaust gas cleaning, and even in the treatment of cells and tissues.

Vibrational excitation of molecules usually makes the most important contribution in the plasma-based chemical kinetics due to the high energy (1 eV) of the plasma electrons delivering the majority of the energy in gases such as N_2 , CO, CO_2 , H_2 e.a. into vibrational excitation. Modulation of plasma-based chemical kinetics via vibrational excitation allows for achieving the ultimate values of energy efficiency. Electrical excitation of gas molecules may also play a substantial role, particularly when the excited molecule lifetime is extremely long. Thus, we can say plasma-produced excited oxygen gas molecules $O_2(^1\Delta_g)$, efficiently contribute to the plasma-based modification of materials and biomedical applications.

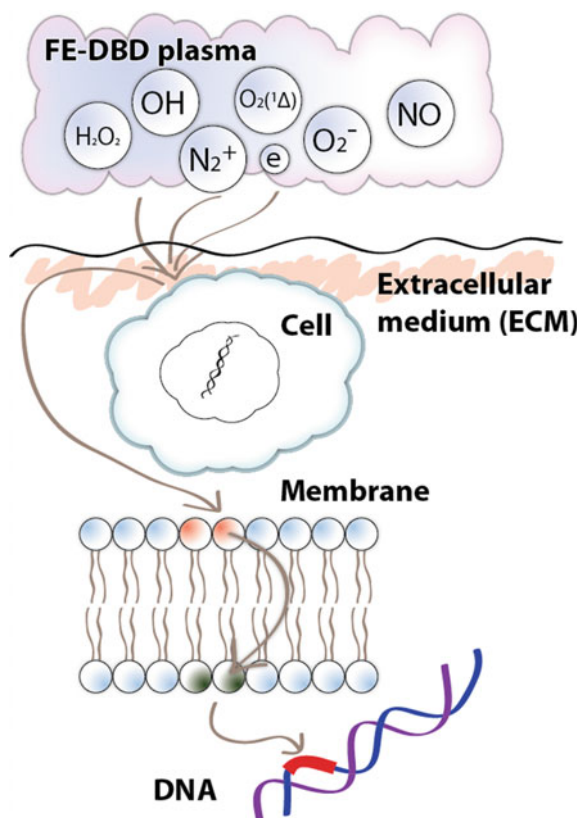
The role of atoms and radicals is noticeably important. Thus, we can point out that oxygen atoms and hydroxyl radicals efficiently produced in air plasma discharges can perform crucial functions in several plasma-based oxidation processes. Photons generated by the plasma discharges as well perform significant roles in many utilizations from plasma-based light sources to water sterilization.

Plasma is also a multi-parametric system together with a multicomponent system, although it is far from thermodynamic equilibrium. Cold plasma discharges are usually strong non-equilibrium systems. Concentrations of the reactive species explained previous text can surpass several orders of magnitude than attained in quasi-equilibrium systems at a similar gas temperature. Effective control of discharge allows the direction of the chemical and biological process in the desired way, selectively, and via the best mechanism. Regulation of plasma-based chemical kinetics required a thorough knowledge of fundamental processes and kinetics of the discharges.

As it was described previously, plasma-based chemical kinetics mechanisms are quite complicated. While there is no doubt that, the level of complexity is way higher in the case of plasma-based interactions with cells and tissues. The simplest

method to approach this complex is to compare biological results of plasma, which are under the not very old fundamental scientific research, with ionizing radiation (IR). From the first look, there is a basic similarity between the molecular effect of IR and nonthermal plasma. Important to note that both affect biomolecules and organisms via the production of ROS. But there are also key differences in the biological mechanisms induced by IR and cold plasma. Importantly, cold plasma can produce several crucial active species that IR does not. Active species generated by plasma includes reactive oxygen and nitrogen species, high level of ions, and strong electric fields. Therefore, investigating the mechanism of the cold plasma treatment must include characterizing the impacts of other species too. More remarkably, IR is high-energy penetrating radiation that produces reactive oxygen species within cells and to a certain extent triggers immediate damage to cells. Nonthermal plasma, on the contrary, does not directly produce reactive species intracellularly. It acts by stimulating reaction chains that start in the plasma discharge. Then the effect of plasma progresses via the extracellular medium altering biomolecules and initiating molecular signaling, diffusing via cell membrane to generate noticeable impacts on living organisms (Fig. 1.6).

Fig. 1.6 Nonthermal plasma-induced bio-molecular processes: Plasma components diffuse via a membrane from the extracellular media leading to intracellular biological effects



The plasma-medical effect can be analyzed for simplicity as three phases demonstrated in Fig. 1.6 where primary reactive species are produced inside of plasma (first phase). Next, the reactive species are transferred from the gas phase into the liquid phase, finally, the reactive species reach biological cells and activate extremely complex intracellular biochemical processes via various molecular signaling (third phase).

1.1.6 Applied Plasma Medicine

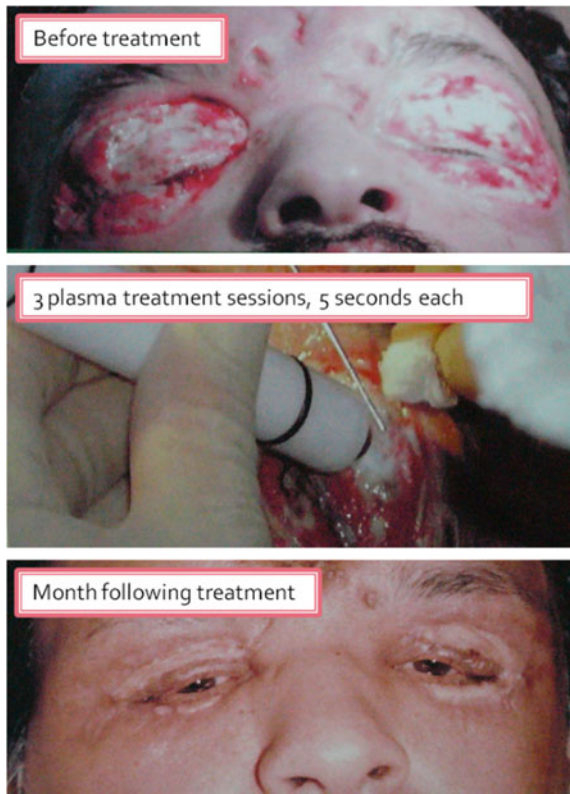
In many applications, nonthermal plasma technologies effectively compete with traditional methods, such as fuel conversion, combustion, coatings, water purification, cleaning of exhaust gases, etc. These plasma applications are fascinating, commercially feasible and usually have made a significant impact on the progress of our society. There is no competition or analogies of the most exciting applications of nonthermal plasma. The plasma abilities in microelectronics processing are exceptional and distinctive. We would not have realized advanced computer systems and mobiles without using plasma. Plasma stays a feasible and effective technology over other traditional strategies. Tuning of plasma's physical properties allows plasma to meet challenges and resolve issues that cannot be resolved in traditional strategies. In some cases, plasma processes are not very efficient, but exceptionally distinctive. Such as other technologies cannot compete with ozone production by plasma (for a century); definitely, we must think about thermonuclear plasma as a distinctive most important energy source.

Similarly, plasma technology attracts considerable attention these days because of opportunities to resolve clinical issues not solved yet, because of the possibilities of treatment of disorders not efficiently treated earlier. The application of cold plasma is capable to shift the paradigm in the medicine area. Those are hopes motivating both fundamental plasma biology and applied to plasma medicine. In ancient times, the application of plasma in the clinical field depends on the thermal effect of discharges for tissue ablation, disinfection etc. Electrocautery is a new method that utilizes regulated heat based on the current passing through the surface of the tissue. However, there is a drawback of this technology treated tissue sometimes adhered to the electrode and causes bleeding again. Plasma can be utilized as an option over electrocautery technology. In case of coagulation, highly conductive plasma is utilized for avoiding the difficulties in tissue adhesion. Thermal plasma is used to cut tissue or skin, though the exact mechanism remains under investigation. Plasma-based thermal effects have also been utilized lately for aesthetic purposes. The main difference in recent applications of plasma over older ones is the utilization of cold discharge effects. Cold plasma is an exciting and encouraging approach to plasma medicine. The key explanation is that cold plasma-based outcomes can be controlled for various biomedical purposes, for example, genetic transfection, cell differentiation or activation, etc. Furthermore, cold plasma can be selective in attaining a required outcome, with little or no side effects. That is why the recent

applications such as coagulation and microbial inactivation which does not affect surrounding cells and tissue.

A lot of specific cases show the efficacy of plasma-based wound healing and treatments of various diseases demonstrated. One interesting case of plasma medicine is related to plasma corneal infections treatment, a case when a patient life has been saved as an outcome of plasma exposure. For this situation, a unique micro-plasma source has been built by Dr. Dobrynin and Dr. Gostev for local treatment of skin diseases, and corneal infections. They investigated thoroughly the effect of plasma against bacteria and corneal infection *in vitro* and *in vivo* utilizing micro-plasma treatment. The experiments confirm the effective bactericidal impact of this plasma discharge with negligible changes to surrounding cells or tissue including delicate cornea tissues. In this study on plasma-based treatment of corneal infection on rabbit cornea, two crucial observations made: (1) plasma exposure showed immediate and efficient bacteria inactivation effect, and (2) This plasma exposure also improved wound healing and regeneration of tissues process. This investigation presented a solid ground for an effective application plasma for the treatment of human patient with complex corneal infection and wounds (Fig. 1.7).

Fig. 1.7 The outcome of treatment (before—on top, after—on bottom) of plasma exposure (shown in the middle) of the complicated ulcerated eyelid wound (in a middle)



Necrotic phlegm on the upper eyelid exposed by air gas plasma for 5s after every few days. After two exposure sessions, the inflammation and edema decreased; and after the third 5s session the plasma exposed area was patient is almost cured and a regenerated tissue appeared. After the 6th session of plasma treatment, the patient was discharged from the hospital (Fig. 1.7). These facts on the first thrilling and inspiring investigation in the applied plasma medicine lead to an opportune moment to take a step from the introduction to the following chapters dedicated to the biomedical area.

As was mentioned, detailed information on plasma medicine fundamentals and applications and especially on the first successful steps in plasma-medical technology can be found in the major reviews and books of Fridman et al. [2], Laroussi et al. [3], Fridman and Friedman [1], Metelmann et al. [4], Toyokuni et al. [5], Keidar et al. [6], Kuo [7], Lu et al. [8], Keidar [9].

1.2 Plasma for Cancer Therapy

1.2.1 Background

Nonthermal atmospheric pressure plasma (NAP) could also called cold plasma is emerging as a promising innovative modality for cancer therapy [6–9]. Cold plasma action is exemplified in several ways, that are mainly related to active species generated in plasma and plasma-based electromagnetic fields by hitting target tissue. The main hypothesis of plasma interaction with biological targets is based on the view constituents of plasma are possibly cytotoxic, like ROS, which may stimulate a “cancer-killing,” but RNS could show a “wound healing or immune activation” effect. Developing different strategies using tuning of these modalities can offer huge possibilities for targeting various signaling pathways in human cells. To this end, it has been demonstrated that plasma exposure possesses potent abilities to kill cancers in cell culture and animal experiments. Importantly, the same plasma treatment shows no or negligible toxicity to normal cells [9]. All these biological outcomes are related to plasma-based active species chemistry and other physical properties. Although the role of active species generated by plasma for cancer treatment described several times, however effects of charged particles and an electric field are not properly investigated. Recent evidence suggests that physical factors such as electromagnetic fields might play an important role [10–14]. These recent observations suggest that multiple chemical and physical modalities exist in cold plasma.

The chemical modality of the cold plasma effect on biological objects is related to active species generation and their transport to the liquid phase from the plasma gas phase and other biological barriers. Several active species generated by plasma are important active constituents in cells [10]. It has been debated that the similarity between plasma active species and biologically generated species signifies the main

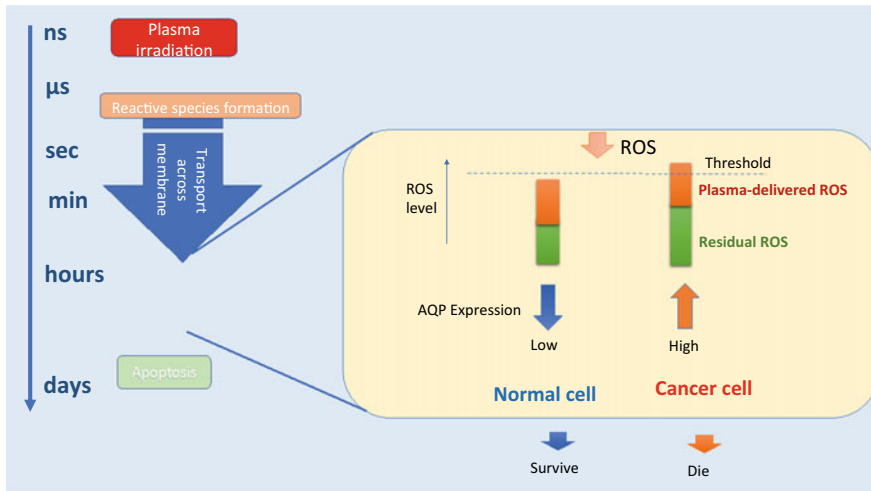


Fig. 1.8 Schematics of plasma interactions at multiscale levels. The magnified insert shows the schematic representation of the plasma interaction with cells explaining selectivity

reason for the application of plasma in cancer treatment and those generated species act as endogenous species in cells [10]. Plasma-generated reactive species show a significant role in ‘redox’ biology [1].

The outline of plasma interaction with biological objects and schematics explaining selectivity is shown in Fig. 1.8. One can see that plasma action is a multi-scale transfer process traversing from the plasma generation at the nano to micro-second, followed by reactive species generation and transport at the timescale of seconds to minutes, ultimately initiating various signaling process inside cells at hours and days.

Several main biological functions are related to active species. For instance, Watson [11] indicated that reactive species are a “positive force for life” because of their function in cell death processes such as apoptosis. concurrently, reactive species are also well known “for their capability to permanently damage many crucial genetic materials and proteins” As such, inside a healthy normal cell reactive species levels are managed by the anti-oxidant machinery. To this end, Watson noticed that “Mostly all physical or chemical agents such as ionizing radiations, and chemical drugs for direct killing cancers, act through by generating ROS that inhibits important cell cycle steps”.

The influence of reactive species on cell processes depends on their levels [12]. Reactive species at less amount can initiate proliferation of cells and support basic cellular functions whereas a high amount of reactive species triggers oxidative stress which may responsible for cell death. Normal cellular function is well-maintained by antioxidant machinery that controls reactive oxygen species levels at a bearable level. A high amount of endogenous reactive species is generated due to the metabolic activity of cancers [12]. To survive, cancer cell alters themselves to control these

species levels. Though, a raise in the reactive species levels inside cells might cause irreversible genomic damage [15]. Concurrently, the level of reactive species in cancer cells is near the threshold limit. Important to note that reactive species level is usually lower in the case of normal cells [15]. Hence, selectivity toward cancer cells oxidative therapy is attained when treatment generated reactive species near the threshold level. This hypothesis is shown schematically in Fig. 1.8.

The reactive oxygen species–based approach is important to plasma-based anti-cancer treatments. Reactive species produced by plasma might initiate apoptosis or autophagy by altering the role of intracellular factors [16]. Conclusively several investigations showed that biologically active reactive oxygen species are generated by plasma such as OH, O, O (1D), $O_2(^1\Delta_g)$, O_3 , HO_2 , and H_2O_2 [17]. Reactive nitrogen species such as NO_2^- , NO^- , and NO^+ are generated directly during the discharge in a gas phase and the plasma-treated media [18].

It should be pointed out that one of the plasma-generated long-lived key species is hydrogen peroxide inside the media [19, 20]. The transport of hydrogen peroxide as well as other ROS is facilitated by cell membrane transport channels such as aquaporins [20, 21]. Multiple studies suggest that tumor cells have more aquaporins than their normal counterpart. Therefore, the transport of hydrogen peroxide is very high in the case of cancer cells through the cell membranes than in normal healthy cells. Such difference in the transport of hydrogen peroxide and rate of consumption might be the potential mechanism of plasma-based cancer treatment. An increase in the reactive species due to the transport of species across cell membranes is related to plasma-generated research species generation outside the cells. An intracellular enzyme such as catalase major factor to control the level of hydrogen peroxide in living cells [22]. It is recently described that the rate of hydrogen peroxide consumption and catalase activity correlate in many cancer and normal cell lines.

1.2.2 In Vivo Applications

Over the last decade, many in vivo investigations have been executed to obtain the anti-cancer impact of cold plasma exposure. In most studies, plasma treatments were carried out by exposing the skin to cancers. Nevertheless, in many investigations, micro-plasma sources were used to direct the microscopic plasma jets to influence the treated cancer below the skin or the cranium [23–25]. All prior investigations described the potential influence of cold plasma on cancer progression.

The initial animal studies were executed by Vandamme et al. [23–25]. They utilized the brain cancer xenograft mice model to assess the anti-cancer outcomes of cold plasma exposure. This groundbreaking study showed a substantial reduction (56%) of tumor volume in the mice exposed to the pulsed floating electrode DBD. The exposed mice survival rate is enhanced by 60% after exposure to the FE-DBD. In this investigation, both tumor volume detection and bioimaging have been utilized to evaluate the cancer inhibition effect of plasma exposure. In this investigation, it is shown that fractioned doses of plasma exposure are much better than a single

long exposure. These kinds of strategies are also famous in the case of radiation biology. Plasma treatments in fractions were further used in several investigations for the treatment of cancers (Fig. 1.9a). Subsequently, the investigation of bladder cancer treatment in xenograft mice models using jet plasma treatment (Fig. 1.9b) was executed [25]. Plasma exposure for 2 min reduced the tumor size significantly. Additionally, researchers executed comparable investigations on skin cancer in a mice xenograft model and attained encouraging outcomes that cancer is inhibited fully after 21 days of plasma exposure. Likewise, the subsequent survival rate is enhanced in the murine model after plasma exposure.

These initial investigations reveal the encouraging capability of plasma exposure as a cancer treatment strategy with no or negligible side effects. Additionally, the same kind of cancer inhibitory effect has been noticed in several other investigations on xenograft animal models. Overall, about 27 *in vivo* investigations have been recognized and concluded the reduction of tumor size and survival rate improvement [27]. It is important to note that all *in vivo* investigations for plasma therapy against cancer are mainly executed on xenograft mice models.

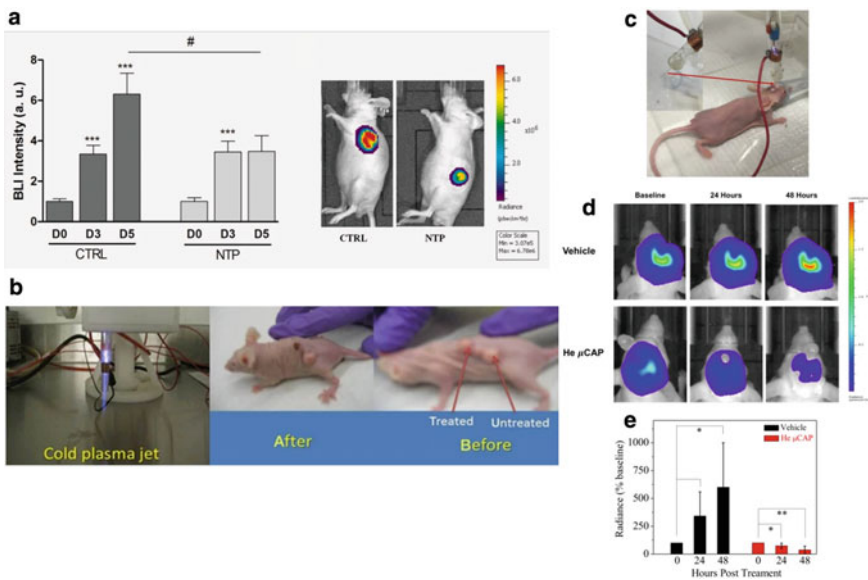


Fig. 1.9 a The initial animal studies for cancer treatment using cold plasma. Once the tumor attained $150 \pm 50 \text{ mm}^3$ sizes, plasma exposure is given to a 6 min plasma exposure (frequency 200 Hz) group in fraction for 5 days. **a** Bioluminescence imaging before plasma exposure (Day 0), in between the treatment period (Day 3), and 24 h after the last treatment (Day 5). **b** Characteristic imaging of untreated control and plasma exposed on the 5th day [24]. **b** Jet plasma and control and plasma treated mice images with multiple tumors (shown after 24 h) [25]. **c** Treatment of glioblastoma with μ -plasma. Image displaying plasma transport via an intracranial endoscopic tube; **d** Images of cancer volume; **e** Outline of radiance intensity helium gas treatment as vehicle and plasma exposure [26]

To investigate the anticancer effect of plasma exposure on glioblastoma a microplasma source is developed. Also, the first intracranial mouse model was used in this plasma-based treatment strategy. The plasma source directly delivers active species to brain cancer using the endoscopic tube for the first time in the plasma medicine area, as shown in Fig. 1.1c [26]. In this investigation cancer volume was measured by a real-time bio-imaging method as shown in Fig. 1.1d. The outcome of these investigations indicated that the cancer volume enhanced only by 50% in the case of the treatment group which is much lower as compared to the untreated control which is 600% after 2 days, as shown in Fig. 1.1e.

To further understand the penetration of reactive agents, EM waves, and plasma species through the skin and scalp, the potential anti-tumor properties of CAP jet non-invasive in an intracranial model have been investigated [28]. To this end, the sensitization effect of a combination of CAP + TMZ was also studied. It has been shown that the jet plasma can seep into the bone, together with active species for plasma strategy over chemotherapy. In this investigation, brain cancer cells were implanted intracranially and allowed to proliferate for 1 week. Consequently, the skull is exposed to the jet plasma directly for 1 min at 1 L per minute helium gas, 12.5 kHz frequency, and 10 V with a 1 cm of distance. Further, TMZ is an anticancer drug injected immediately at a 6 mg/kg/day dose for 2 weeks. Anticancer drug TMZ alone did not inhibit cancer growth (Fig. 1.10a, b), due to resistance of cancer against TMZ exposure as earlier reported. However, one dose of plasma exposure alleviated the cancer growth by 40% compared to control, although this did not reach statistical significance (Fig. 1.10a, b). Importantly, a combination of plasma and TMZ potentially inhibited brain cancer progression in this investigation (Fig. 1.10a, b). Altogether, these outcomes indicate that: (1) The jet plasma can penetrate the biological barriers, and (2) A single plasma exposure sensitizes brain cancers to successive anticancer drug TMZ treatment.

1.2.3 Clinical Studies

In 2017, the outline of the first medical investigation was reported [28–30]. The clinical trial registered six patients with advanced (pT4) squamous cell carcinoma of the oropharynx with open infected ulcers. Patients were exposed to jet plasma for 3 times treatments in 3 weeks, each treatment followed by an interval of a week. Plasma exposure triggers a decrease in odor and pain medicine necessity, which enhanced the social activity of patients and initiated an encouraging emotional impact. The partial relapse of cancer in 2 patients within 9 months has been detected. In a biopsy, enough amount of cancer apoptotic cells and desmoplasia were observed in the surrounding tissue. This medical investigation underlines the medical importance and prospective plasma treatment could have in clinical oncotherapy going forward. In general, the medical utilization of potential strategies in other areas of oncology is presently under examination. Plasma-induced cancer inhibition is a potential outcome that will be investigated further In the United States, Keidar et al. George Washington

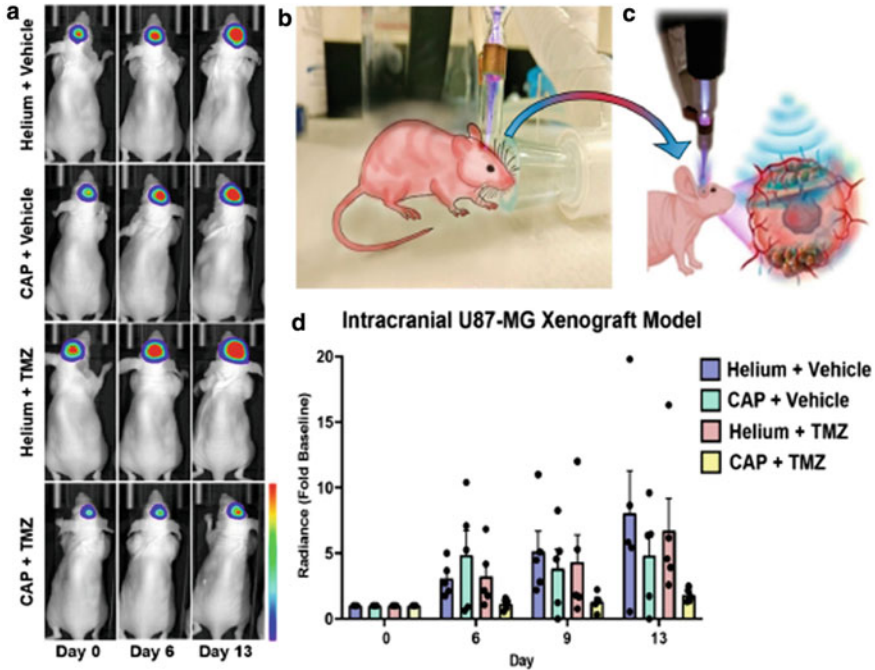


Fig. 1.10 **a** Characteristic BLI images at initial time (day 0) and 6 and 13 days after plasma exposure with or with anticancer drug TMZ injection. **b** Graphic description of the plasma treatment to mice model and **c** penetration of electromagnetic waves across the skin and cranium to kill brain cancer. **d** Outline of emitted radiance throughout the investigation

University together with US Medical Innovation conducted a medical application by treating remaining cancerous tissue without affecting normal cells after surgery of the final stage of colon cancer in a patient in 2015. Next, this group together with the Canady group used Canady Helios plasma source and plasma scalpels in the clinical liver resection to remove and kill remaining cancer cells. Very recently the US Food and Drug Administration has given authorization for 25 patients to undergo plasma treatment as an adjunct therapy to treat tumors [31]. Achieving additional awareness into plasma acceptable side effect summary along with its efficacy as the selective anticancer agent will steer more clinical trials.

1.3 Non-thermal Atmospheric Pressure Plasma Diagnostics

1.3.1 Optical Emission Spectroscopy (OES) for Plasma

In PBRC, the collision radiation models were used for Ar and nitrogen plasmas to obtain plasma temperatures and densities of atmospheric plasmas. In the case of Ar plasma, we referred to simple Ar collisional radiative (CR) model [32, 33]. This can be exploited to investigate the electron temperature of nonthermal plasma by optical emission spectroscopy (OES) with four metastable Ar state intensities. This method is assumed that the plasma follows a Maxwell-Boltzmann distribution and experiment emission intensities are used for determination of an electron temperature and the excited Ar atom densities. The reference [33] considered excited processes only from metastable state denoted by $1s_3$ and $1s_5$ to $2p$ excited levels denoted by $2p_1 \sim 2p_{10}$ in CR model. But the excited processes from resonance states denoted by $1s_2$ and $1s_4$ to $2p$ energy levels should not be ignored because these processes must occur in atmospheric pressure plasma [34]. We propose the modified CR model by inclusion of these resonant excited processes for accurate determination of electron temperature for atmospheric pressure plasma jet [35]. For N_2 (or air) plasma, we referred the collisional radiative model of nitrogen gas [36] for obtaining the electron temperature and density. It is included the physical processes from the ground state $X^1\Sigma_g^+$ to the excited states $A^3\Sigma_u^+$, $B^3\Pi_g$ and $C^3\Pi_u$ [37].

The impact excitation of Ar plasma by electron can be described as the populations of the $2p$ excited Ar states are made by electron collisions from Ar atoms in ground to excited states of the metastable and resonance states. Our CR model included the excited processes of the resonance and metastable states and we selected eight $2p$ emission lines for solving the balance equations. The modified equation for a $2p_x$ in Paschen notation excited level can be written by inclusion of resonant states ($i = 2, 4$) along with metastable states ($i = 3, 5$) in left hand side of Eq. (1.1), as,

$$n_e n_g k_{g,2p_x} + \sum_{i=2,3,4,5} n_e n_{1s_i} k_{1s_i,2p_x} = \sum_{i=2,3,4,5} n_{2p_x} A_{2p_x,1s_i} \quad (1.1)$$

where n denotes number density (n_e : electron density, n_g : neutral gas density, n_{1s_i} : $1s_i$ level density, n_{2p_x} : $2p$ level density), $k_{1s_i,2p_x}$ is the excitation rate coefficient from level $1s_i$ to $2p_x$, which depend on the electron temperature, and $A_{2p_x,1s_i}$ is the transition probability from level $2p_x$ to $1s_i$. The subscript g stands for ground level, e for electrons, and $1s_i$ and $2p_x$ are the Paschen notations [33]. The relative number density for specified wavelength could be represented by the optical emission intensities measured from spectrometer. For example, the n_{2p_x} can be written as in Eq. (1.2),

$$n_{2p_x} \approx \frac{I_{2p_x-1s_i} \lambda_{2p_x-1s_i}}{A_{2p_x-1s_i}} \quad (1.2)$$

where I is the measured optical emission intensity, and λ the given wavelength [33]. Equation (1.3) can be used in Eq. (1.2) to replace n_{2p_x} and Eq. (1.1) can be rewritten by following [33]

$$n_e = \frac{\sum_{i=5}^2 n_{2p_x} A_{2p_x, 1s_i}}{n_g k_{g, 2p_x} + \sum_{i=2,3,4,5} n_{1s_i} k_{1s_i, 2p_x}} \quad (1.3)$$

This equation can be expressed by the measured intensity for any $2p_x$ level of $2p_1$ (750.387 nm), $2p_3$ (706.722 nm), $2p_4$ (794.850 nm), $2p_5$ (751.500 nm), $2p_6$ (763.510 nm), $2p_7$ (810.040 nm), $2p_8$ (842.600 nm) and $2p_9$ (811.531 nm) occurred by the electron impact excitation in Ar plasma. Because the excited atom density n_{2p_x} is expressed as the relative intensity, the electron density n_e can be the relative values. It is the same to each other for eight $2p_x$ levels. We can establish 4 equations depended on electron temperatures with unknown variable of excited atom densities $1s_2$, $1s_3$, $1s_4$ and $1s_5$. The Ar excited 1s atom densities can be solved for all electron temperatures by using mathematical python library. The electron density in Eq. (1.3) can be written by these specific 1s densities depended on the electron temperature. By comparing the two selected electron density equations, it is possible to obtain a section in which the values are the same at a specific electron temperature. This electron temperature at this time becomes the value we are looking for. This method can find the electron temperature and excited 1s atom densities in atmospheric pressure Ar plasma.

Figure 1.11 shows the process of OES diagnostics method by using Ar emission eight lines in nonthermal atmospheric pressure Ar plasma. This method can be used for the determination of electron temperature and excited atom densities ($1s_2$, $1s_3$, $1s_4$, $1s_5$) of Ar plasma. In the atmospheric pressure Ar plasma, we measured the Ar I emission lines and, as applying Ar CR model, the electron temperature was 1.28 eV, the excited Ar $1s_2$, $1s_3$, $1s_4$ and $1s_5$ densities were $1.92 \times 10^{15} \text{ cm}^{-3}$, $4.03 \times 10^{15} \text{ cm}^{-3}$, $1.88 \times 10^{15} \text{ cm}^{-3}$, and $5.79 \times 10^{15} \text{ cm}^{-3}$, respectively.

In an air (or nitrogen) plasma, we basically used nitrogen molecule collisional radiative model of reference [35–39]. The ground state $X^1\Sigma_g^+$ can be transitioned to the excited upper states $A^3\Sigma_u^+$, $B^3\Pi_g$, and $C^3\Pi_u$ by the electron impact effect of plasma [35–39]. And the excited nitrogen molecules in the A and B states could be exchanged by collision with N_2 molecules in the state $X^1\Sigma_g^+$, respectively [35–39]. Nitrogen molecules in lower states $A^3\Sigma_u^+$ and $B^3\Pi_g$ are corresponding to spontaneous emission from higher states $B^3\Pi_g$ and $C^3\Pi_u$, from which the spectra of N_2 FPS (first positive system) and N_2 SPS (second positive system) are emitted [35–39]. And, the excited molecule of $A^3\Sigma_u^+$ state can have the wall deactivation [35–39]. In addition, for practical application to atmospheric plasma, we need to consider the energy pooling reaction, which represents the transition to the $B^3\Pi_g$, $C^3\Pi_u$, and $X^1\Sigma_g^+$ states due to the collision between two molecules in the $A^3\Sigma_u^+$ state [35–39]. Therefore, we can develop the total balance equations for these excited $A^3\Sigma_u^+$, $B^3\Pi_g$, and $C^3\Pi_u$ state [35–39].

In the case of N_2 (A),

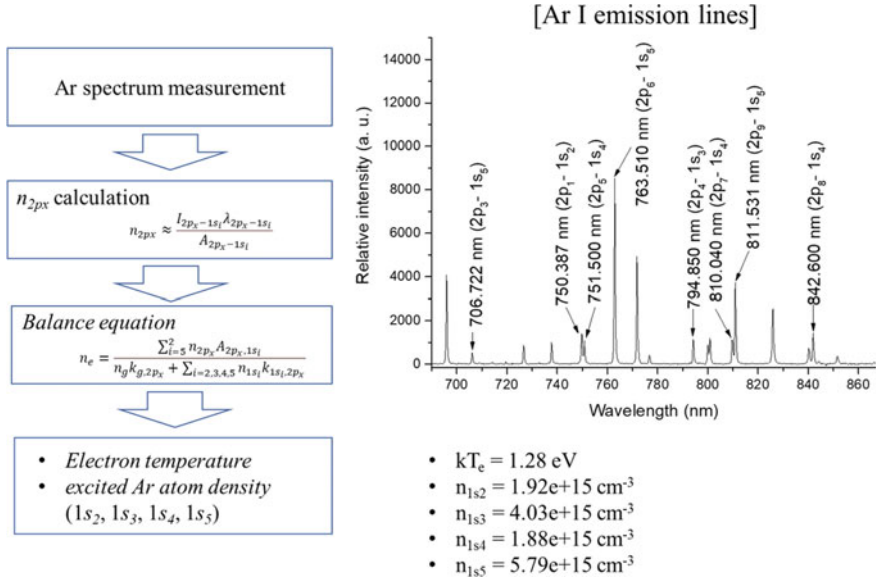


Fig. 1.11 OES diagnostics process of Ar emission lines in atmospheric pressure Ar plasma

$$2n_A^2(k_{AAB} + k_{AAC}) + (k_{\text{wall}} + k_{AX}n_v)n_A - (A_B + k_{BX}n_g)n_B - n_e n_g Q_A = 0 \quad (1.4)$$

In the case of N_2 (B),

$$n_A^2 k_{AAB} + k_{AX} n_v n_A - (A_B + k_{BX} n_g) n_B + A_C n_C + n_e n_g Q_B = 0 \quad (1.5)$$

In the case of N_2 (C),

$$n_A^2 k_{AAC} - A_C n_C + n_e n_g Q_C = 0 \quad (1.6)$$

The n_e , n_A , n_B , and n_C are the density of electron and excited states $A^3\Sigma_u^+$, $B^3\Pi_g$, and $C^3\Pi_u$, respectively. The n_v and n_g are the neutral gas densities for vibrational temperature and ground state depending on the gas temperature. The k_{AX} and k_{BX} are the rate coefficients for transition processes between $A^3\Sigma_u^+ - X^1\Sigma_{g^+}$ and $B^3\Pi_g - X^1\Sigma_{g^+}$ states, respectively [37]. The k_{AAB} and k_{AAC} are the rate coefficients for the transition process to upper states $B^3\Pi_g$ and $C^3\Pi_u$ after the collision with excited states $A^3\Sigma_u^+$ [37]. The k_{wall} is the wall deactivation rate coefficient that is derived by the diffusion model with the wall reflection [37]. The Q_A , Q_B , and Q_C are the rate coefficients from the ground to excited states $A^3\Sigma_u^+$, $B^3\Pi_g$, and $C^3\Pi_u$, respectively, caused by electron impact excitation [31, 37]. The A_B and A_C are the transition probabilities of excited states $B^3\Pi_g$ and $C^3\Pi_u$ [37].

We could obtain three 2nd order balance equations for three unknown variables of excited densities n_A , n_B , and n_C in Eqs. (1.4)–(1.6). These excited molecule densities for N_2 can be solved simply using mathematical library in python software. Also, we can express the excited molecule densities by assigning an arbitrary electron temperature and density into Eqs. (1.4)–(1.6). The ratio of molecule densities for N_2 SPS and FPS can be written as belows [37],

$$R(kT_e, n_e) = \frac{A_C n_C}{A_B n_B} \quad (1.7)$$

The magnitudes of Eq. (1.7) could be compared by measured ratio of emission intensities between N_2 SPS and FPS, which depend on the electron temperatures and densities. N_2 SPS emission lines could be selected to be the wavelength of 295.3, 313.6, 315.9, 337.1, 353.7, 357.7, 371.1, 375.5, 380.5, 389.5, 399.8, and 405.9 nm [32]. Also, N_2 FPS intensity could be selected to be the wavelength of 654.5 nm [32]. We can find the 12 lines ratio R values, which depended on the arbitrary electron temperature and density, for 12 lines of N_2 SPS and one line of FPS in atmospheric pressure air plasma. The specific electron temperature can be obtained by comparing with measured emission line ratio in OES data of air plasma. These electron temperatures can be expressed according to arbitrary electron densities and obtained for each 12 lines ratio. We can find a specific electron density with the same electron temperature.

Figure 1.12 shows the process of OES diagnostics method by using N_2 emission lines in nonthermal atmospheric pressure air plasma. This method can be used for obtaining the electron temperature and density, rotational and vibrational temperature, and excited N_2 molecule densities (n_A , n_B , n_C) of air plasma. The line ratios of the intensity N_2 plasma were measured and the estimated line ratio between N_2 SPS and FPS can be calculated by using the balance equations of nitrogen collisional radiative model. By comparing these values, the various plasma parameters can be solved in atmospheric pressure air plasma. In the case of plasma temperature in air plasma, the electron, rotation and vibration temperature had values of 1.05 eV, 847.60 k, and 0.76 eV, respectively. Also, in the case of plasma density, the electron, N_2 molecule densities of the excited states A, B, and C had values of $1.12 \times 10^{15} \text{ cm}^{-3}$, $9.78 \times 10^{15} \text{ cm}^{-3}$, $1.31 \times 10^{16} \text{ cm}^{-3}$, and $1.72 \times 10^{15} \text{ cm}^{-3}$, respectively.

Table 1.1 has shown the arrangement for plasma parameters that can be calculated with the collisional radiative model of atmospheric pressure Ar and N_2 plasma.

1.3.2 Measurement of the Electron Density by Using Optical Interferometer

Electron densities which is important parameter of great interest in plasma are responsible for the generation of reactive oxygen or nitrogen species used for industrial, agricultural and medicine processes. But, electron density measurement for weak

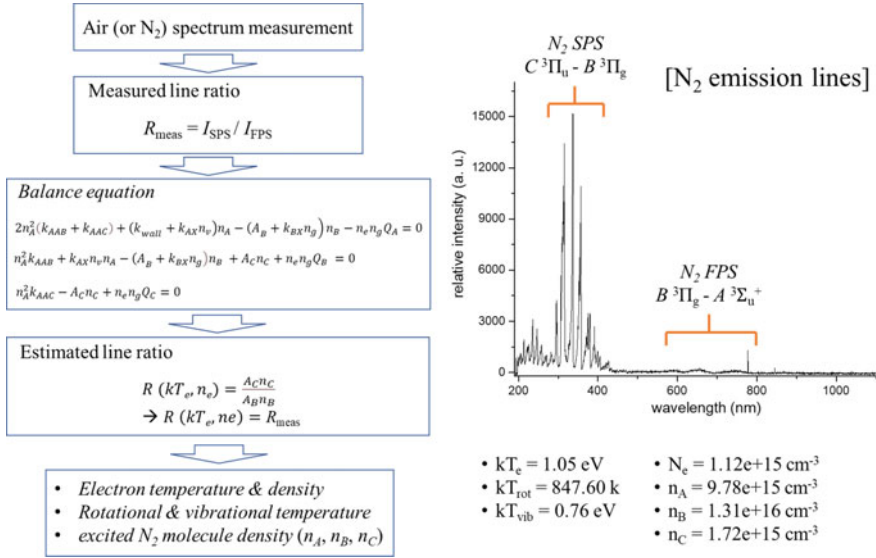


Fig. 1.12 OES diagnostics process of N_2 emission lines in atmospheric pressure Air plasma

Table 1.1 Comparing with Ar and N_2 collisional radiative model

Parameters	Ar CR model	N_2 CR model
Plasma temperature	<ul style="list-style-type: none"> Electron temperature 	<ul style="list-style-type: none"> Electron temperature Vibrational temperature Rotational temperature
Plasma density	<ul style="list-style-type: none"> Excited Ar atom density ($1s_2, 1s_3, 1s_4, 1s_5$) 	<ul style="list-style-type: none"> Electron density Excited N_2 molecule density (n_A, n_B, n_C)

ionized plasmas such as atmospheric pressure dielectric barrier discharge (DBD) plasma jet and DBD surface plasma are easily perturbed by small interferences, so diagnosis for electron density is mainly performed by indirect optical methods such as laser interferometry, optical emission spectroscopy, and Thomson scattering [35–41]. Laser interferometers offer the advantages of responsiveness to rapid discharge and the ability to tune sensitivity of electron density by changing the probing laser wavelength. The plasma electron density could be calculated by refractive index obtained from measured laser phase shift [37–41]. In this chapter, we introduce the Michelson interferometry system which perform laser phase shift measurement for estimation of electron density from a plasma without heterodyne system.

Figure 1.13 shows the Michelson interferometry for the plasma electron density measurement. Here M1 to M4 are optical mirrors, BS is a beam splitter, BE is a beam expander, LPF is a line-pass filter (for corresponding to probing laser wavelength of

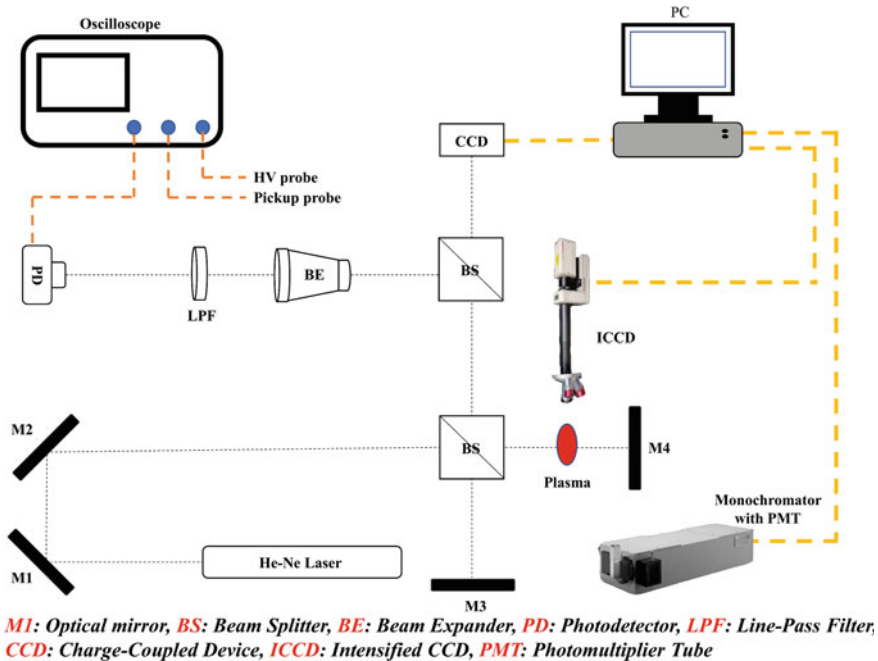


Fig. 1.13 Michelson interferometry for the plasma electron density measurement [43]

632.2 nm), PD is photodetector and CCD is a charge-coupled device. From this interferometry, the phase shift of the laser beam is caused by the optical path difference. The interferogram line intensity I could be denoted by the following equation:

$$I = \frac{I_0}{2} [1 + \cos(k\Delta z + \Delta\varphi)], \tag{1.8}$$

where, I_0 is the initial laser beam intensity prior to division by the beam splitter, k is the wave number, $\Delta\varphi$ is the optical phase difference, and Δz is the optical path difference between the two mirror arms for M3 and M4. The interferent lines consist of constructive and destructive patterns with phases of $2m\pi$ and $(2m - 1)\pi$, ($m = 1, 2, 3, \dots$), respectively, as determined by Eq. (1.8).

Figure 1.14a shows a CCD image for the laser interferent fringes. The relative intensities of the fringes representing constructive and destructive interference are represented by the photodetector signal intensities (in volts) as shown in Fig. 1.14b. The signal of interference pattern would could be shifted from bright (constructive) to dark (destructive) or dark to bright one in this photodetector by change in optical path difference, which has been done by fine adjustment of interferometry mirror (M3 or M4) in Fig. 1.13. From the line shift signals, we can obtain the phase shift of laser interferogram due to the plasma which installed on the fixed mirror arm [41]. This phase shift, $(n - 1)\frac{2\pi}{\lambda}d$, associated with refractive index n , plasma's electron

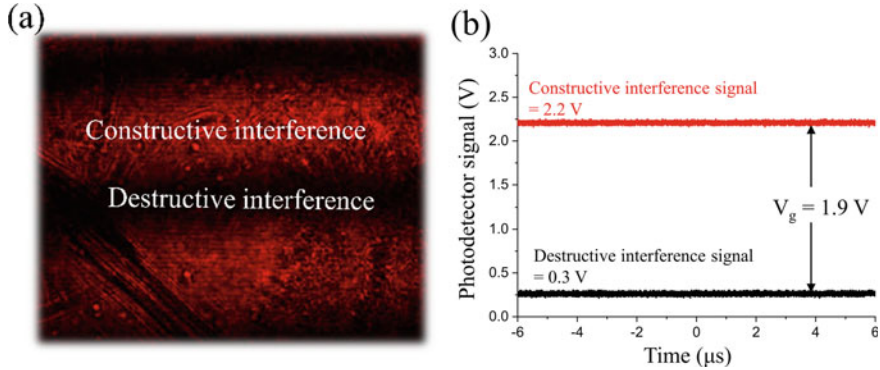


Fig. 1.14 **a** CCD image of interferent fringes with constructive and destructive patterns. **b** Measured photodetector signals in both interferent patterns [43]

density N_e and heavy particle density N_{heavy} is given by the following equation [42]:

$$(n - 1) \frac{2\pi}{\lambda} d = -\frac{e^2 \lambda d}{4\pi c^2 m_e \epsilon_0} N_e + \frac{2\pi d}{\lambda} A \left(1 + \frac{B}{\lambda^2} \right) \frac{N_{\text{heavy}}}{N_{\text{heavy}0}}, \quad (1.9)$$

where m_e is the electron mass in kg, λ is the laser wavelength in m, ϵ_0 is the permittivity in vacuum in F/m, c is the speed of light in m/s, and d is the laser path in the plasma region in m, which is twice the plasma width because the laser has double transit path from the mirror (M4) to the beam splitter (BS). Further, N_{heavy} and $N_{\text{heavy}0}$ are the densities in m^{-3} of heavy particles (ions, molecules, neutral atoms) in plasma state and initial state, respectively, under room temperature and pressure ($T = 290$ K, $p = 1$ atm). A and B in the second term of right hand side are specific coefficients for heavy particle species [42, 44]. The optical path of the laser beam causes phase shift in the interferogram lines since the refractive index has been changed by plasma.. The slope of phase shift for electron density is very greater than that of heavy particles' one in the atmospheric pressure discharge and heavy mass (72,872 times larger than electron mass in case of argon plasma) [41]. The photodetector signal of phase shift by electron density (ΔV_e), which is caused by fast electrons in the plasma, can be measured by a spatially fixed photodetector. V_g is the gap voltage between constructive and destructive interference. Therefore, the relation of phase shift ($\Delta\varphi$) in Eq. (1.8) between before and after discharge, which can be written as [43]

$$\Delta\varphi = \cos^{-1} \left(\frac{2(V_e - V_d)}{V_g} - 1 \right) - \cos^{-1} \left(\frac{2(V_I - V_d)}{V_g} - 1 \right), \quad (1.10)$$

where V_I is the initial voltage of photodiode signal before discharge, V_e is the end point voltage of the fast transient signal by plasma electrons after discharge and V_d is the photodiodesignal in destructive interference. For the measured photodiode signal ($\Delta V_e = V_e - V_I$) produced by phase shift ($\Delta\varphi$), the plasma electron density can

be measured from $\Delta\varphi = 2\pi d(n - 1)/\lambda$ and Eq. (1.9) by elimination of the heavy particles. The electron density N_e could be expressed by [43]

$$N_e = \frac{4m_e\epsilon_0\pi c^2}{e^2\lambda d} \left\{ \cos^{-1}\left(\frac{2(V_e - V_d)}{V_g} - 1\right) - \cos^{-1}\left(\frac{2(V_l - V_d)}{V_g} - 1\right) \right\} [\text{m}^{-3}]. \tag{1.11}$$

The maximum electron density is limited by the V_g value of 1.9 V in this measurement, which corresponds to π radian in phase shift. Therefore, the maximum electron density can be measured to be $5.5 \times 10^{18} \text{ cm}^{-3}$ in this experiment from Eq. (1.11) under $V_g = 1.9 \text{ V}$, $d = 320 \text{ }\mu\text{m}$, and $\Delta V_e = V_g$.

Figure 1.15a, b show the interferogram brightness change by transient spark discharge. After discharge, destructive interference line of interferogram has been changed to constructive interference line by spatial plasma refractive index change. Figure 1.15c shows the total variation of interferogram line intensity, it was increased with discharge from initial level of photodetector signal and restored to initial level after few \sim ms. It means that spatial refractive index has been changed by plasma electron density and heavy particle. An initial increase of photodetector signal shows distinguishable slope difference in Fig. 1.15d. Initial increase of photodiode signal, $\Delta V_e + \Delta V_h$, contains both electron and heavy particle effects with slope of $2.94 \text{ mV}/\mu\text{s}$, and late signal ΔV_h contains only heavy particle effect with slope of $0.44 \text{ mV}/\mu\text{s}$, respectively. From these experimental measurement, the electron density could be estimated to be $8.5 \times 10^{15} \text{ cm}^{-3}$ by Eq. (1.11) by taking into account only the electron slope, $2.50 \text{ mV}/\mu\text{s}$, which can be obtained by subtracting the slope caused by the heavy particle from the initial slope in photodiode signal.

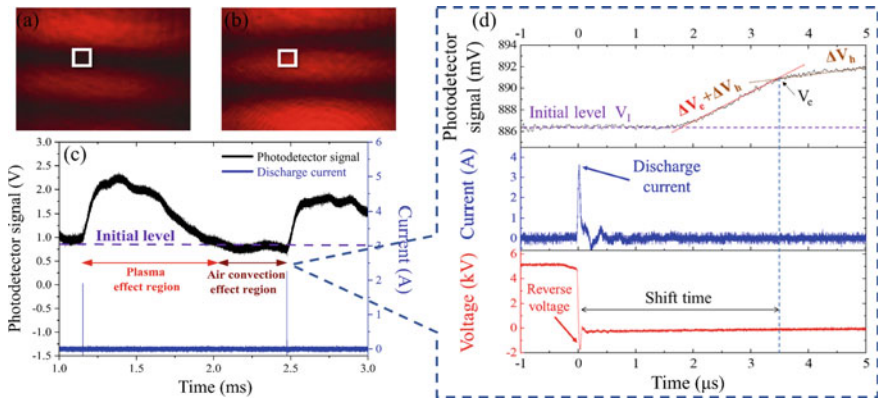


Fig. 1.15 **a** Laser interference pattern before discharge, **b** after discharge (white squares are photodiode sensitive area), **c** Transient photodiode signal (black line) with spark discharge current (blue line). **d** Photodiode signal $\Delta V_e + \Delta V_h$ from plasma electrons and heavy particles with fast slope, and signal ΔV_h from heavy particle with slow slope (top) with voltage (middle) and current (bottom) signal in time [43]

1.3.3 Measurement of the Plasma Radicals by Using Ultraviolet Absorption Spectroscopy

Reactive species in cold atmospheric pressure plasma play an important role in biomedical fields and industry. Because an cold air plasma can generate many kinds of reactive species, the generation of radical species is an important issue for the plasma device. The ultraviolet(UV) diagnostics of the cold plasma is very important to measure the density of reactive species. Also many researchers have widely used ultraviolet absorption pectroscopyin density measurement of reactive species.

The hydroxyl radicals OH of ROS (reactive oxygen species) can be measured by the ultraviolet absorption spectroscopy in CAP plasma. The experimental configuration of this absorption spectroscopy has been represented in references [45, 46]. This setupconsists of the UV lamp, in which a Hg lamp has been used with its power of 0.5 W, centered at 306 nm, and plano-convex lens whose wavelength ranges from ultraviolet to infrared are transmitted [45]. The UV light has been transmitted and focused to the 200 um in diameter in the plasma jet by using the plano-convex lens for UV absorption measurement for the OH species occurred at 307 ~ 309 nm [45]. The Lambert-Beer's law can estimate the density of hydroxyl OH radical species in CAP with UV absorption spectroscopy. The intensity for the incident and transmitted UV light through the plasma region whose thickness is x , are represented to be I_o and I_v , respectively. The density of hydroxyl OH radical species produced by the CAP jet is given by [45]

$$N = -\frac{1}{\sigma \cdot x} \ln\left(\frac{I_v}{I_o}\right) \quad (1.12)$$

where N is the hydroxyl OH density, and σ is the collisional cross-section of about $6 \times 10^{-11} \text{ m}^2$ for OH species [47], and x is 300 μm . The hydroxyl OH radical density could be estimated by Eq. (1.12) from the experimental measurement of I_v/I_o i.e., ratio of the transmitted intensity through the plasma to incident one at wavelengths of 307 ~ 309 nm.

Figure 1.16a The strong UV absorption profile can be seen at wavelenths about 309 nm in the transmitted signal (I_v) through the plasma (black color line), which is caused by the OH radical species of Ar CAP jet, whose gas flow rates are ranged from 80 to 300 sccm [46]. The incident intensity of UV lamp (I_o) and emission intensity from OH radical species in the CAP jet without UV incidence have been denoted by red and blue lines, respectively, in Fig. 1.16a. The UV emission from the plasma and absorption lines at about 309 nm caused by OH radicals are denoted by the circles in the blue line and the dotted box in the black one, respectively, as shown in Fig. 1.16a [46]. The transmission ratio (I_v/I_o) of UV signals can be converted the OH density at the absorbed wavelength of about 309 nm. Figure 1.16b shows the density of OH radical species at 2 mm over the interfacial water surface versus the Ar gas flow rate from 80 to 240 sccm, where electrical power is 15 W and the driving frequency is 22 kHz [46]. The OH density reaches the maximum to be $2.6 \times 10^{15} \text{ cm}^{-3}$ under the

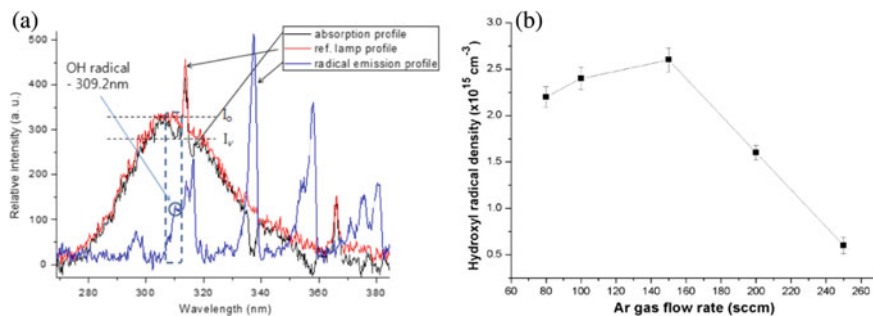


Fig. 1.16 **a** UV transmitted profile (I_v) through the plasma jet (black), in which absorption occurred at wavelengths of 307 ~ 309 nm, caused by the OH radical species. Reference UV lamp profile (I_0) versus the wavelength without nonthermal atmospheric pressure plasma jet (red). Optical emission profiles from the plasma jet versus the wavelength (blue) without UV incidence. **b** Hydroxyl OH radical density at the interfacial water surface region contacted by plasma, which is 2 mm above the water surface versus the Ar gas flow rates from 80 to 240 sccm [45]

gas flow rate of ~ 150 sccm and it is rapidly decreased to $6.0 \times 10^{14} \text{ cm}^{-3}$ for ~ 250 sccm in this report [46].

For the density measurement of the reactive nitrogen species (NO_x), the cavity-enhanced absorption spectroscopy (CEAS) or Fourier Transform Infrared (FTIR) spectroscopy methods are widely used [48]. For nitrogen dioxide (NO_2) measurement, the visible broad band cavity-enhanced absorption spectroscopy (BBCEAS) method could be used [48]. However, for density measurement of nitric oxide (NO), CEAS should be used for diagnostics of infrared-active molecules by using a mid-infrared laser, whose spectral range is between 3 and 20 μm [49]. The NO_2 absorption profile could be obtained by using UV and visible light sources such as light emitting diode (LED) and Xe or Hg arc lamps. The absorption band of NO_2 molecule includes the electronic transition band in the visible spectra [50]. However, the vibronic absorption band of NO species is located around infrared 5.26 μm and its absorption profile can be detected by a quantum cascade laser (QCL). This kind of NO absorption spectroscopy has been used generally and the QCL can be adjusted to a specific laser wavelength [50]. The BBCEAS and QCL-CEAS techniques could be used well frequently for density measurements of NO_2 and NO respectively, based on these reasons [64]. In this chapter, we describe the density measurement of NO_2 and NO generated by air NAP jet by employing the BBCEAS with LED and CEAS with QCL [51]. For the measurement of NO_2 and NO density, a visible LED (660 nm) and a mid-infrared laser diode (LD) (5.2386 μm) could be used, respectively [51]. These radical densities could be measured by using Beer-Lambert law, Eq. (1.12), which is obtained by the absorbed laser intensity passing through the plasma gas region inside an optical cavity of CEAS [51]. We obtain the NO_2 density to be $\sim 2.5 \times 10^{16} \text{ cm}^{-3}$ in air plasma et. and Also NO density has a value of $\sim 4 \times 10^{15} \text{ cm}^{-3}$ [51] in recent report [51]. To find the NO maximum absorption wavelength the transmission ratio (I_v/I_0) has been measured in the QCL's tunable wavelength ranges [51]. Figure 1.17a

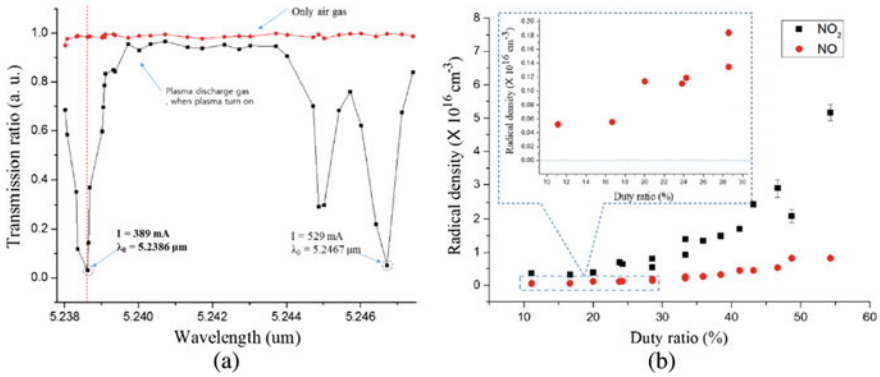


Fig. 1.17 **a** The transmission ratio of mid-infrared LD beam for NO density measurement versus wavelength of QCL, **b** NO₂ (black) and NO (red) radical densities versus the duty ratio (%)

shows the absorption wavelength 5.2386 μm corresponding to the NO’s first peak of absorption [51]. Figure 1.17b shows the densities of NO₂ and NO reactive species in the air NAP jet versus pulse duty ratio [51].

1.3.4 Plasma Parameter Characteristics for Industry and Biomedical Plasma Products

In PBRC (Plasma Bioscience Research Center) of Kwangwoon university, Korea, various plasma biomedical devices have been developed and studied about plasma parameters, plasma density and temperature [46]. For these parameters, we applied to the nitrogen collisional radiative (CR) model with OES data of NAP or CAP [52]. The nitrogen OES can be obtained based on the CR model for the determination of plasma temperatures (electron temperature, rotational and vibrational temperature) and densities (electron density, and excited nitrogen molecule densities) [53]. The OES intensities from the N₂ second positive system (SPS) and first positive system (FPS) are very important in modelling the N₂ CR model, by which the plasma temperatures and plasma densities could be estimated in nonthermal atmospheric pressure plasma [16]. These physical properties are provided by PBRC to a Korean and foreign companies for supplying various plasma products. These physical parameters could be used as evidence for plasma being used for various purposes as well as basic data for performance evaluation.

Figure 1.18 shows that PBRC plasma sources can be largely classified into plasma jet and surface DBD plasma type. Plasma jet is suitable for the treatment of local treatment area in human body (teeth, skin wound) or material sample. On the other hand, surface DBD plasma could be is used for large area plasma processing purposes. In particular, the surface DBD type is divided into three categories, where counter or facing-DBD, coplanar-DBD and floating electrode—DBD. The plasma parameters

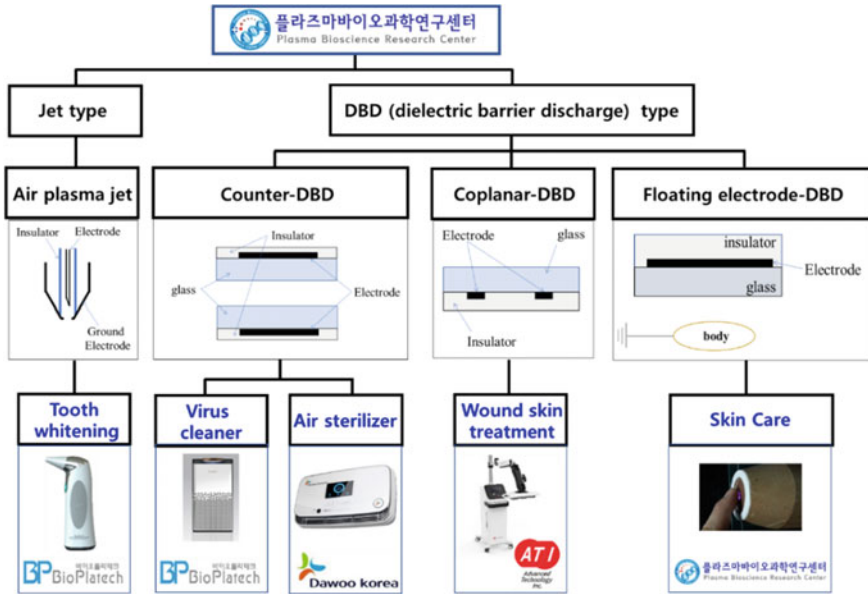


Fig. 1.18 The plasma biomedical devices developed in PBRC of Kwangwoon university

(electron density and temperature, vibrational and rotational temperature, excited nitrogen molecule densities n_A , n_B , and n_C) could be investigated through N_2 CR model for PBRC plasma sources.

The air plasma jet consists of a needle-shaped electrode, a ground electrode covered around the outside, and a glass tube that insulates central power electrode. This technology is currently applied as a plasma tooth whitening device through technical transfer to “Bio-Platech” company, and its development has been completed and is on marketing sale. The counter or facing—DBD is a structure in which two glass substrates printed by electrode material and then covered with dielectric materials, respectively, and then they are installed by facing each other with a finite separation distance, as shown in Fig. 1.18. Plasma discharge occurs in the space between glass substrates by applying opposite polarity to each counter electrode. This plasma source is currently used in the virus cleaner and air sterilizer products. We have completed commercial product development in cooperation with “Bio-Platech” and “Dawoo Korea” company. The coplanar-DBD is a surface discharged structure consisting of two electrodes covered with insulator on a glass substrate. The plasma discharge occurs on insulator surface by applying opposite polarity to each electrode in coplanar surface, as shown in Fig. 1.18. Currently, this technology is developing for the wound skin treatment medical devices in hospital through “ATI” company. The structure of the floating electrode—DBD is similar to that of the counter-DBD except counter substrate with counter electrode. Here, the human body could be grounded as a counter electrode and only homopolar voltage signal has been put onto the floating DBD electrode. Hence the plasma discharge occurs

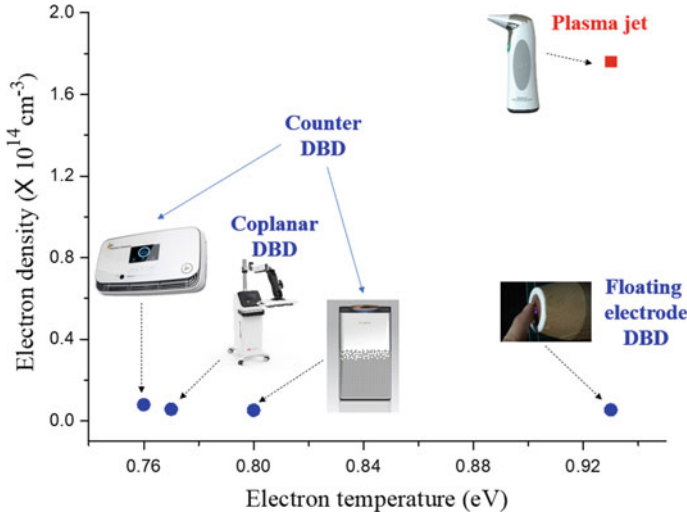


Fig. 1.19 Mapping of electron density and temperature in biomedical plasma devices

in a space between the floating-DBD surface and body. It can be used for skin care medical device since this plasma can directly contact on skin surface.

Figure 1.19 shows the mapping for electron density and electron temperature, which are obtained from the nitrogen CR model for PBRC plasma sources. The electron temperature and density are found to be maximum of 0.93 eV and $1.76 \times 10^{14} \text{ cm}^{-3}$ in air plasma jet. The electron temperature of floating electrode-DBD is higher than that of other DBD sources. Also, the electron density shows that they are in the ranges of $\sim 10^{12} \text{ cm}^{-3}$ in DBD type.

The rotational and vibrational temperature of the plasma jet and DBD plasma type are shown in Fig. 1.20. Here these plasma rotational and vibrational temperatures are shown to be more than twice those of the DBD type. The rotational and vibrational temperature of the jet type are approximately maximum of 712 K and 0.76 eV, respectively. In the case of surface DBD plasma, the average value for rotational and vibrational temperature are shown to be 350 K and 0.35 eV, respectively, which are about half of that of jet type.

For the excited nitrogen molecule, N_2 , density is shown in Fig. 1.21, where n_A is higher than n_B , n_C for all types of plasma sources. Here n_A , n_B , and n_C denote the N_2 molecular densities for excited energy states of $A^3\Sigma_u^+$, $B^3\Pi_g$, and $C^3\Pi_u$, respectively. At the plasma jet, the order of n_A is similar to n_B , but in the case of DBD, n_A is higher than other species. In plasma jet type, the excited molecule densities have the ranges between 10^{14} and 10^{15} cm^{-3} , also DBD type has the ranges between 10^{12} and 10^{14} cm^{-3} .

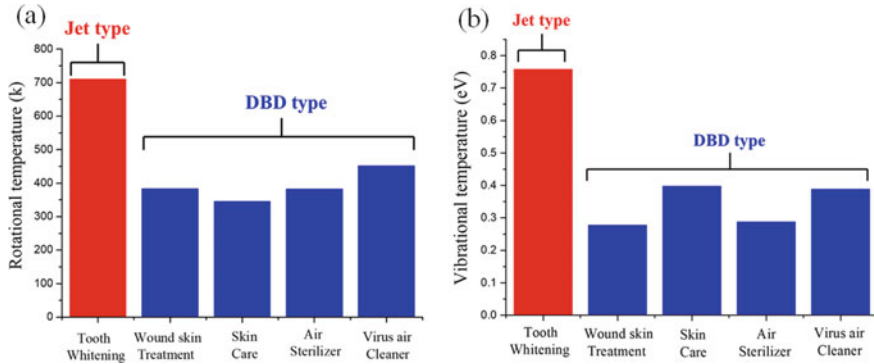


Fig. 1.20 a The rotational and b vibrational temperature for plasma biomedical devices

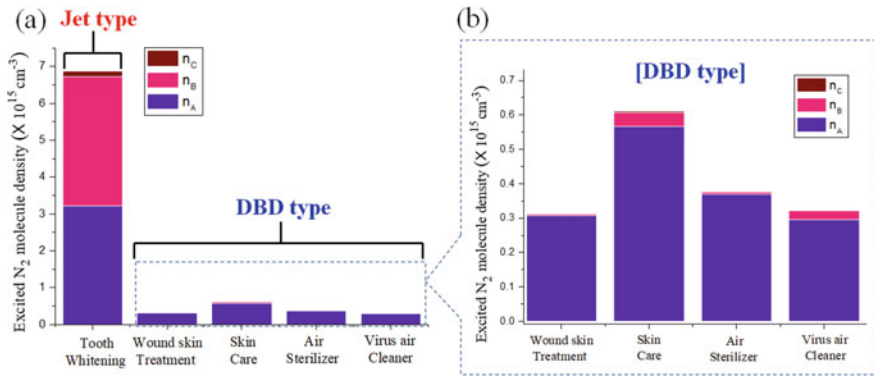


Fig. 1.21 a The excited N₂ molecule density of plasma jet and surface DBD plasma type and b expanded excited N₂ molecule density of surface DBD plasma type for biomedical devices

Acknowledgements This work was supported by the Korean National Research Foundation (2021R1A6A1A03038785).

References

1. A. Fridman, G. Friedman, *Plasma Medicine* (Wiley, UK, 2013)
2. G. Fridman, G. Friedman, A. Gutsol et al., Applied plasma medicine. *Plasma Process. Polym.* **5**(6), 503–533
3. M. Laroussi, M. Kong, G. Morfill, W. Stolz (eds.), *Plasma Medicine* (Cambridge University Press, N.Y, 2012)
4. H.-R. Metelmann, T. von Woedke, K.-D. Weltmann (eds.), *Comprehensive Clinical Plasma Medicine* (Springer, Berlin, Germany, 2018)
5. S. Toyokuni, Y. Ikehara, F. Kikkawa (eds.), *Plasma Medical Science* (Elsevier, Academic Press, UK, USA, 2018)

6. M. Keidar, D. Yan, J. Sherman, *Cold Plasma Cancer Therapy* (IOP e-books, 2019)
7. S. Kuo, *Cold Atmospheric Plasmas, Their Use in Biology and Medicine*, (World Scientific Publications, 2019).
8. X.P.Lu, S. Reuter, M. Laroussi, D.W.Liu, *Non-Equilibrium Atmospheric Pressure Plasma Jets: fundamentals, Diagnostics, and Medical Applications* (CRC Press, Taylor & Francis, 2019)
9. M. Keidar (ed.), *Plasma Cancer Therapy* (Springer, Berlin, Germany, 2020)
10. D. Graves, J. Phys. D: Appl. Phys. **45**, 263001 (2012)
11. J. Watson, Perspective: oxidants, antioxidants and the current incurability of metastatic cancers. *Open Biol.* **3**, 120144 (2013)
12. R. Cairns, I. Harris, T.W. Mak, Regulation of cancer cell metabolism. *Nat. Rev. Cancer* **11**, 85–95 (2011)
13. D. Yan., Q. Wang, M. Adhikari, A. Malyavko, L. Lin, D. B. Zolotukhin, X. Yao, M. Kirschner, J. Sherman, M. Keidar, A physically triggered cell death via transbarrier cold atmospheric plasma cancer treatment. *ACS appl. Mater. interfaces.* **12**(31), 34548–34563 (2020)
14. X. Yao, D. Yan, L. Lin, J. Sherman, K. Peters, S. Keir, M. Keidar, Cold plasma discharge tube enhances anti-tumoral efficacy of temozolomide. *ACS Appl. Bio Mater.* **5**(4), 1610–1623 (2022)
15. D. Trachootham, J. Alexandre, P. Huang. *Nat. Rev. Drug Discov.* **8**, 579–591 (2009)
16. E.A. Ratovitski, X. Cheng, D. Yan, J.H. Sherman, J. Canady, B. Trink, M. Keidar, Anti-cancer therapies of 21-st century. Novel approach to treat human cancers using cold atmospheric plasma. *Plasma Process. Polym.* **11**, 1128–1137 (2014)
17. G. Manda, M.T. Nechifor, T.-M. Neagu, Reactive oxygen species, cancer and anti-cancer therapies. *Curr. Chem. Biol.* **3**(1), 22–46 (2009)
18. P. Lukes, E. Dolezalova, I. Sisrova, M. Clupek, *Plasma Sour. Sci. Technol.* **23**, 015019 (2014)
19. N. Kurake, H. Tanaka, K. Ishikawa, T. Kondo, M. Sekine, K. Nakamura, H. Kajiyama, F. Kikkawa, M. Mizuno, M. Hori, Cell survival of glioblastoma grown in medium containing hydrogen peroxide and/or nitrite, or in plasma-activated medium. *Arch. Biochem. Biophys.* **605**, 102–108 (2016)
20. D. Yan, A. Talbot, N. Nourmohammadi, J. Sherman, X. Cheng, M. Keidar, Toward understanding the selectivanti-cancer capacity of cold atmospheric plasma—A model based on aquaporins. *Biointephases* **10**, 040801 (2015)
21. D. Yan, H. Xiao, W. Zhu, N. Nourmohammadi, L.G. Zhang, K. Bian, M. Keidar, The role of aquaporins in the anti-glioblastoma capacity of the cold plasma-stimulated medium. *J. Phys. D: Appl. Phys.* **50**(055401), 2017 (2016)
22. C.M. Doskey, V. Buranasudja, B.A. Wagner, J.G. Wilkes, J. Du, J.J. Cullen, G.R. Buettner, *Redox Biol.* **10**, 274–284 (2016)
23. M. Vandamme, E. Robert, S. Pesnel, E. Barbosa, S. Dozias, J. Sobilo, S. Lerondel, A. Le Pape, J.M. Pouvesle, Antitumor effect of plasma treatment on U87 glioma xenografts: preliminary results. *Plasma Process. Polym.* **7**, 264 (2010)
24. M. Vandamme, E. Robert, S. Lerondel, V. Sarron, D. Ries, S. Dozias, J. Sobilo, D. Gosset, C. Kieda, B. Legrain, J.-M. Pouvesle, A. Le Pape, ROS implication in a new antitumor strategy based on non-thermal plasma. *Int. J. Cancer* **130**, 2185 (2011)
25. M. Keidar, R. Walk, A. Shashurin, P. Srinivasan, A. Sandler, S. Dasgupta, R. Ravi, R. Guerrero-Preston, B. Trink, Cold plasma selectivity and the possibility of a paradigm shift in cancer therapy. *Br. J. Cancer* **105**, 1295 (2011)
26. Z. Chen, H. Simonyan, X. Cheng, L. Lin, J. Canady, J.H. Sherman, M. Keidar, A novel micro cold atmospheric plasma device for glioblastoma both in vitro and in vivo. *Cancers* **9**(6), 61 (2017)
27. A. Dubuc, P. Monsarrat, F. Virard, N. Merbahi, J.-P. Sarrette, S. Laurencin-Dalicieux, S. Cousty, Use of cold-atmospheric plasma in oncology: a concise systematic review. *Ther. Adv. Med. Oncol.* **10**, 1–12 (2018)
28. V. Soni, M. Adhikari, H. Simonyan, L. Lin, J.H. Sherman, C.N. Young, M. Keidar, In vitro and in vivo enhancement of temozolomide effect in human glioblastoma by non-invasive application of cold atmospheric plasma. *Cancers* **13**(17), 4485 (2021)

29. H.-R. Metelmann, C. Seebauer, V. Miller et al., Clinical experience with cold plasma in the treatment of locally advanced head and neck cancer. *Clin Plasma Med* **9**, 6–13 (2018)
30. H.-R. Metelmann, T. von Woedtke, K.D. Weltmann, *Comprehensive Clinical Plasma Medicine: cold Physical Plasma for Medical Application* (Springer), pp. 185–195
31. <https://www.businesswire.com/news/home/20190731005521/en/USMI-JCRI-ABTS-Receive-FDA-Approval-Conduct-U.S>
32. D. Mariotti, Y. Shimizu, T. Sasaki, N. Koshizaki, Method to determine argon metastable number density and plasma electron temperature from spectral emission originating from four 4p argon levels. *Appl. Phys. Lett.* **89**, 201502 (2006)
33. J.S. Lim, R.H. Kim, Y.J. Hong, P. Lamichhane, B.C. Adhikari, J. Choi, E.H. Choi, Interactions between atmospheric pressure plasma jet and deionized water surface. *Results Phys.* **19**, 103569 (2020)
34. X. Zhu, Y. Pu, A simple collisional-radiative model for low-temperature argon discharges with pressure ranging from 1 Pa to atmospheric pressure: kinetics of Paschen 1s and 2p levels. *J. Phys. D: Appl. Phys.* **43**, 015204 (2010)
35. X.-M. Zhu, Y.-K. Pu, Optical emission spectroscopy in low-temperature plasmas containing argon and nitrogen: determination of the electron temperature and density by the line-ratio method. *J. Phys. D: Appl. Phys.* **43**, 403001
36. X.-M. Zhu, P. Yi-Kang, Determination the electron temperature in inductively coupled nitrogen plasmas by optical emission spectroscopy with molecular kinetic effects. *Phys. Plasmas* **12**, 103501 (2005)
37. J. T. Gudmundsson, Electron excitation rate coefficients for the nitrogen discharge. *Sci. Inst. Univ. Iceland, Reykjavik, Iceland, Tech. Rep. RH-09-2005* (2005)
38. A. Ortiz-Mora, A. Díaz-Soriano, A. Sarsa, M.S. Dimitrijević, C. Yubero, A practical method for plasma diagnosis with Balmer series hydrogen lines. *Spectrochim Acta Part B* **163**, 105728 (2020)
39. K. Urabe, H. Muneoka, S. Stauss, K. Terashima, Microscopic heterodyne interferometry for determination of electron density in high-pressure microplasma. *Plasma Sour. Sci. Technol.* **23**(6), 064007 (2014)
40. K. Urabe, H. Muneoka, S. Stauss, K. Terashima, Development of near-infrared laser heterodyne interferometry for diagnostics of electron and gas number densities in microplasmas. *Appl. Phys. Exp.* **6**, 126101 (2013)
41. J.C. Rost, E.M. Davis, A. Marinoni, M. Porkolab, M.A.V. Zeeland, A combined phase contrast imaging and heterodyne interferometer for multiscale fluctuation measurements in tokamak plasmas. *J. Inst.* **14**, C12023 (2019)
42. C.W. Allen, A.N. Cox, *Allen's Astrophysical Quantities* (Springer Science & Business Media, 2001)
43. K.H. Becker, U. Kogelschatz, K.H. Schoenbach, R.J. Barker, *Non-Equilibrium Air Plasmas at Atmospheric Pressure* (CRC Press, 2004)
44. Y.J. Hong, C.J. Nam, K.B. Song, G.S. Cho, H.S. Uhm, D.I. Choi, E.H. Choi, Measurement of hydroxyl radical density generated from the atmospheric pressure bioplasma jet. *J. Instrum.* **7**(03), C03046 (2012)
45. Y.H. Kim, Y.J. Hong, K.Y. Baik, G.C. Kwon, J.J. Choi, G.S. Cho, H.S. Uhm, D.Y. Kim, E.H. Choi, Measurement of reactive hydroxyl radical species inside the biosolutions during non-thermal atmospheric pressure plasma jet bombardment onto the solution. *Plasma Chem. Plasma Process.* **34**(3), 457–472 (2014)
46. H.P. Dorn, R. Neuroth, A. Hofzumahaus, Investigation of OH absorption cross sections of rotational transitions in the band under atmospheric conditions: implications for tropospheric long-path absorption measurements. *J. Geophys. Res.: Atmosp.* **100**(D4), 7397–7409 (1995)
47. G. Berden, R. Engeln, *Cavity Ring-Down Spectroscopy Techniques and Applications* (Wiley, UK 2009), p. 59
48. S. Iseni, S. Reuter, K.-D. Weltmann, NO₂ dynamics of an Ar/Air plasma jet investigated by in situ quantum cascade laser spectroscopy at atmospheric pressure. *J. Phys. D: Appl. Phys* **47**, 075203 (2014)

49. J.P. Burrows, A. Dehn, B. Deters, S. Himmelmann, A. Richter, S. Voigt, J. Orphal, Atmospheric remote-sensing reference data from gome: Part I. temperature-dependent absorption cross-sections of NO₂ in the 231–794 nm range. *J. Quant. Spectrosc. Radiat. Transf.* **60**(6), 1025 (1998)
50. Y.J. Hong, J. Lim, J.S. Choi, K.D. Weltmann, E.H. Choi, Measurement of nitrogen dioxide and nitric oxide densities by using CEAS (cavity-enhanced absorption spectroscopy) in nonthermal atmospheric pressure air plasma. *Plasma Process. Polym.* **18**(1), 2000168 (2021)
51. M. Keidar, D. Yan, J.H. Sherman, *Cold Plasma Cancer Therapy* (Morgan & Claypool Publishers, 2019), pp. 53–73
52. H. Ahn, K. Kim, N. Hoan, C. Kim, E. Moon, K. Choi, S. Yang, J. Lee, *PLoS ONE* **9**, e86173 (2014)
53. D. Trachootham, J. Alexandre, P. Huang, *Nat. Rev. Drug Discov.* **8**, 579–591 (2009)
54. A. Lofthus, P.H. Krupenie, The spectrum of molecular nitrogen. *J. Phys. Chem. Ref. Data* **6**(1), 113–307 (1977)
55. P.J. Ryan, J.W. Bradley, M.D. Bowden, Comparison of Langmuir probe and laser Thomson scattering for plasma density and electron temperature measurements in HiPIMS plasma. *Phys Plasmas* **26**, 040702 (2019)
56. T. Akiyama, M.A. Van Zeeland, R.L. Boivin, T.N. Carlstrom, J.A. Chavez, C.M. Muscatello, R.C. O'Neill, J. Vasquez, M. Watkins, W. Martin, A. Colio, D.K. Finkenthal, D.L. Brower, J. Chen, W.X. Ding, M. Perry, Bench testing of a heterodyne CO₂ laser dispersion interferometer for high temporal resolution plasma density measurements. *Rev. Sci. Instrum.* **27**, 123502 (2016)
57. B. Seo, P.M. Bellan, Spatially translatable optical fiber-coupled heterodyne interferometer. *Rev. Sci. Instrum.* **88**, 123504 (2017)
58. J.S. Lim, Y.J. Hong, B. Ghimire, J. Choi, S. Mumtaz, E.H. Choi, Measurement of electron density in transient spark discharge by simple interferometry. *Results Phys.* **20**, 103693 (2021)
59. D. Yan, A. Talbot, N. Nourmohammadi, X. Cheng, J. Canady, J. Sherman, M. Keidar, Principles of using cold atmospheric plasma stimulated media for cancer treatment. *Sci. Rep.* **5**, 18339 (2015)
60. M. Ishaq, M.D.M. Evans, K.K. Ostrikov, *Biochimica et Biophysica Acta (BBA)-molecular cell research* **1843**(12), 2827–2837 (2014)
61. F. Leipold, R.H. Stark, A. El-Habachi, K.H. Schoenbach, Electron density measurements in an atmospheric pressure air plasma by means of infrared heterodyne interferometry. *J. Phys. D Appl. Phys.* **33**, 2268–2273 (2000)